Low-Cycle Fatigue Behavior of Sn-Ag, Sn-Ag-Cu, and Sn-Ag-Cu-Bi Lead-Free Solders

CHAOSUAN KANCHANOMAI,[1] YUKIO MIYASHITA,[1] and YOSHIHARU MUTOH[1,2]

1.—Department of Mechanical Engineering, Nagaoka University of Technology, Nagaoka 940-2188, Japan. 2.—E-mail address: mutoh@mech.nagaokaut.ac.jp

Low-cycle fatigue (LCF) tests on as-cast Sn-3.5Ag, Sn-3Ag-0.5Cu, Sn-3Ag-0.5Cu-1Bi, and Sn-3Ag-0.5Cu-3Bi solders was carried out using a noncontact strain-controlled system at 20°C with a constant frequency of 0.1 Hz. The addition of Cu does not significantly affect the fatigue life of eutectic Sn-Ag solder. However, the fatigue life was significantly reduced with the addition of Bi. The LCF behavior of all solders followed the Coffin–Manson relationship. The fatigue life of the present solders is dominated by the fracture ductility and can be described by the ductility-modified Coffin–Manson's relationship. Steps at the boundaries of dendrite phases were the initiation sites for microcracks for Sn-3.5Ag, Sn-3Ag-0.5Cu, and Sn-3Ag-0.5Cu-1Bi solders, while for Sn-3Ag-0.5Cu-3Bi solder, cracks initiated along both the dendrite boundaries and subgrain boundaries in the dendrite phases. The linking of these cracks and the propagation of cracks inside the specimen occurred both transgranularly through eutectic phases and intergranularly along dendrite boundaries or subgrain boundaries.

Key words: Low-cycle fatigue, lead-free solder, Sn-3.5Ag, Sn-3Ag-0.5Cu, Sn-3Ag-0.5Cu-1Bi, Sn-3Ag-0.5Cu-3Bi, ductility-modified Coffin–Manson's relationship, crack initiation, crack propagation

INTRODUCTION

In the surface mount technology (SMT) developed for electronic packaging, devices are directly soldered to pads on both sides of a printed wiring board. This technology allows placement of more surface mount components into smaller and tighter printed wiring board areas. However, for SMT, the ability for absorbing the thermal and mechanical strains is degraded. The thermal strain is induced by the mismatch of thermal expansion coefficient between components during processing and in service. Since the solder is softer than other components, most of the damage accumulates in the solder. Therefore, fatigue failure, particularly thermally induced low-cycle fatigue (LCF) failure, can occur in these solders.

There are environmental and health concerns about the hazard of lead contained in conventional solder materials. Lead-free Sn-Ag system solders are candidates for electronic packaging. The mechanical properties of the Sn-Ag eutectic solder compare favorably with those of the Sn-Pb eutectic solder, while the solderability and melting temperatures are less favorable than those of Sn-Pb eutectic solder.[1] In order to improve these properties, some additional elements, e.g., Cu, Bi, Zn, and In, have been added to Sn-Ag eutectic solder. It has been reported that the melting temperatures, i.e., liquidus and solidus temperatures, of Sn-Ag eutectic could be decreased by adding Bi or Zn.[2,3] However, low melting temperature solder would mean higher homologous temperature of service (the ratio between service temperature and melting temperature, in Kelvin), which enhances the occurrence of more thermally activated processes such as creep and grain growth. These thermally activated processes reduce the reliability of the solder joint. Therefore, an understanding of LCF behavior and crack initiation and propagation mechanisms of the eutectic solder with alloying additions is necessary for developing the reliable SMT electronic packaging. Kariya and Otsuka[4,5] reported that the fatigue life of Sn-

(Received October 29, 2001; accepted January 3, 2002)

3.5Ag-Bi for a total axial strain-controlled test decreased with increasing contents of Bi (0–10 wt.%), while addition of Cu (0–2 wt.%) had no effect on the fatigue properties of Sn-3.5Ag-Cu. This reduction is attributed to the decrease in ductility with Bi addition and the presence of irregularly shaped Ag_3Sn in the microstructure. However, very little is known about the characteristics and mechanisms of crack initiation and propagation during LCF in Sn-Ag-Cu and Sn-Ag-Cu-Bi solders.

In the present study, isothermal LCF tests on as-cast Sn-Ag, Sn-Ag-Cu, and Sn-Ag-Cu-Bi solders were carried out to study LCF behavior and mechanisms. In strain-controlled fatigue tests, an extensometer is commonly mounted on the specimen for measuring the displacement of the specimen gage. However, for soft materials such as solders, the local deformation and stress concentration can be induced around the contact point between the extensometer probe and specimen surface. The cracks have a tendency to initiate earlier in this area, reducing the specimen life.[6] To avoid this effect, a noncontact displacement measurement system[7] was used in the strain-controlled fatigue tests on solders.

MATERIALS AND EXPERIMENTAL PROCEDURES

Sn-3.5Ag, Sn-3Ag-0.5Cu, Sn-3Ag-0.5Cu-1Bi, and Sn-3Ag-0.5Cu-3Bi alloys were supplied in as-solidified form. The compositions and liquidus and solidus temperatures of the alloys are listed in Table I. Additions of Cu and Bi reduced the melting temperature of solders when compared to Sn-Ag eutectic solder. The values of solidus decrease with the addition of Bi, while the differences in the liquidus temperature are not significant.

For observation of the microstructures, the solders were etched with 10 g of $FeCl_3$, 2 mL of HCl, and 100 mL of distilled water. Scanning electron microscopy (SEM) micrographs of the alloys are shown in Fig. 1. For the Sn-3.5Ag alloy, β-Sn phase is the major phase, which comprises over 90% by volume. Its microstructure can be characterized by primary β-Sn dendrites (dark) and Sn-Ag eutectic phases (light), as shown in Fig. 1a. The high-magnification micrograph (Fig. 1b) shows the presence of some needles and particles of Ag_3Sn together with the Sn-rich matrix in Sn-Ag eutectic phase. Similar microstructures were observed for Sn-3Ag-0.5Cu, Sn-3Ag-0.5Cu-1Bi, and Sn-3Ag-0.5Cu-3Bi; however, both Ag_3Sn and Cu_6Sn_5 form in the Sn-Ag-Cu eutectic phases (light). According to the binary phase diagrams of Sn-Ag and Sn-Cu,[8] the solubility of Ag and Cu in the Sn-rich phase at eutectic and room temperature is negligible. Therefore, the dendrite structures (dark) of Sn-3.5Ag and Sn-3Ag-0.5Cu are basically pure β-Sn. On the other hand, from the binary phase diagram of Sn-Bi,[8] approximately 1 wt.% and 21 wt.% of Bi can dissolve in the Sn-rich matrix at room temperature and eutectic temperature (139°C), respectively. Therefore, the dendrite phase in Sn-3Ag-0.5Cu-1Bi is essentially the solid solution of Bi in β-Sn unlike the Bi-free solders, which contain β-Sn dendrites. Dendrites in Sn-3Ag-0.5Cu-3Bi solder contain precipitates of Bi in the solid solution of Bi in β-Sn. It has been reported that adding Bi over the solid solubility limit to the Sn-rich alloy results in the crystallization of fine Bi and irregularly shaped Ag_3Sn intermetallics (coarse and platelike) around β-Sn globules containing Ag_3Sn intermetallics.[5]

Monotonic tensile tests were conducted in order to understand the basic mechanical properties. Round specimens with a diameter of 7 mm and gage length of 20 mm were used for the tests. Since time-dependent deformation can occur even at room temperature for the present solders, a strain rate greater than 2×10^{-2} s^{-1} was used to obtain time-independent mechanical properties.[9] For the present study, the strain rate of 4×10^{-2} s^{-1} was used for the tensile tests at 20°C. The mechanical properties of the solders studied are summarized in Table II.

From bulk solder bar materials, fatigue specimens, as shown in Fig. 2, were machined on an NC lathe machine. The configuration of the specimen, which was designed according to the ASTM recommendation,[11] has a diameter of 12 mm at the two ends, a center diameter of 6 mm, and a gage length of 9 mm with a radius of curvature of 20 mm to prevent any stress concentration due to sharp corners. In order to remove the deformation layer due to machining, the gage part of the specimen was electrolytically polished and left to fully age at room temperature for more than 30 days. Cutiongco et al.[12] indicated that fatigue life increased after a day or two of aging and leveled off after a week. Electrolytic etching was performed at room temperature with 8 DC voltage for 3 min in a solution of ethanol (80%) 800 mL, distilled water 140 mL, and perchloric acid (60%) 60 mL. The total strain-controlled fatigue tests were performed by using a servohydraulic fatigue machine with 2 kN load cell under 55% relative humidity and a constant temperature

Table I. Compositions of Lead-Free Solders (Wt.%)

Solder	Sn	Ag	Cu	Bi	Pb	Liquidus (°C)	Solidus (°C)
Sn-3.5Ag	96.5	3.5	—	—	—	221	221
Sn-3Ag-0.5Cu	96.5	3	0.5	—	—	219	217
Sn-3Ag-0.5Cu-1Bi	95.5	3	0.5	1	—	219.5	213
Sn-3Ag-0.5Cu-3Bi	93.5	3	0.5	3	—	219.5	207
Sn-37Pb	63	—	—	—	37	183	183

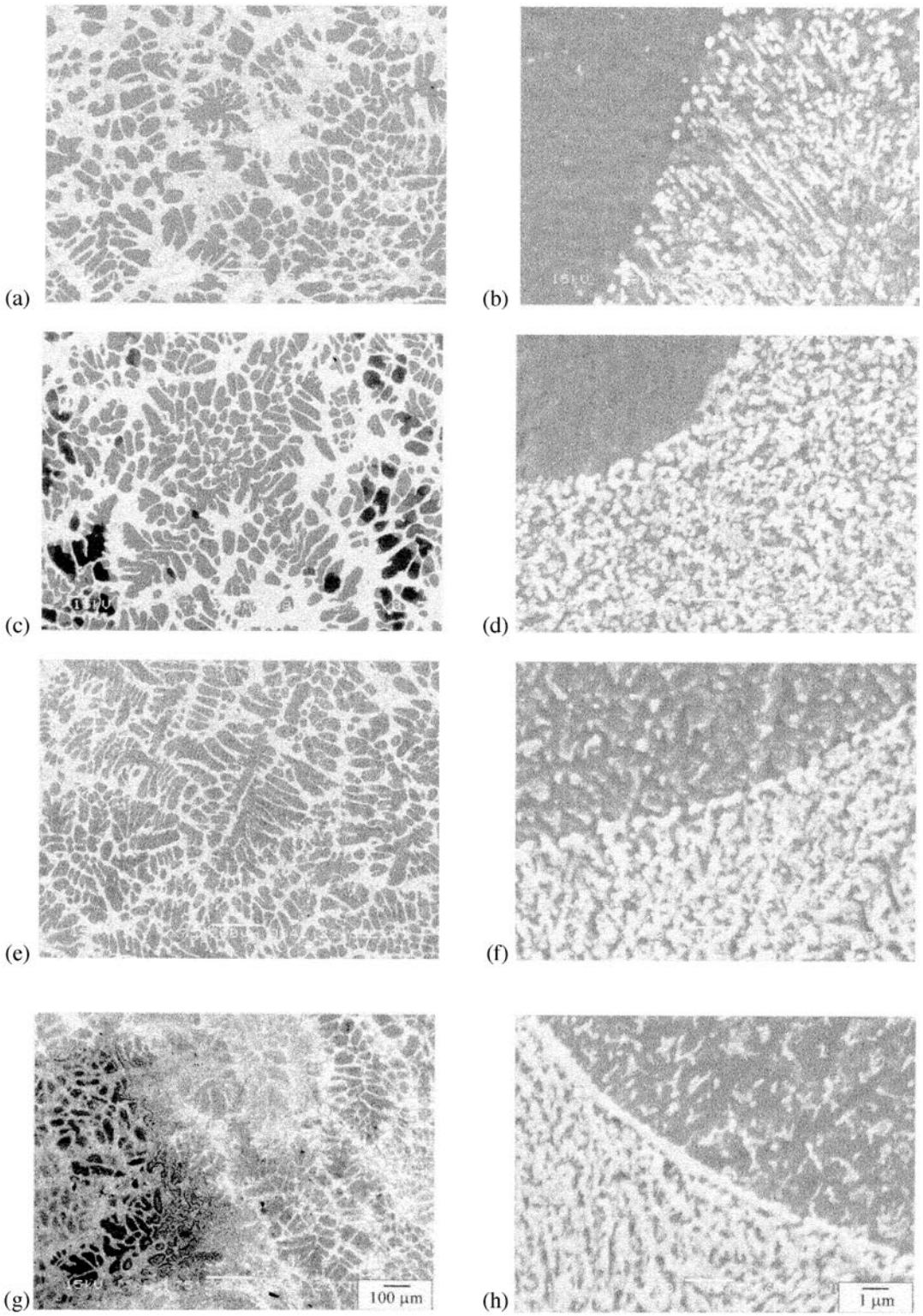

Fig. 1. SEM micrographs of Sn-3.5Ag eutectic solder: (a) low magnification; (b) high magnification, Sn-3Ag-0.5Cu solder; (c) low magnification; (d) high magnification, Sn-3Ag-0.5Cu-1Bi solder; (e) low magnification; (f) high magnification, Sn-3Ag-0.5Cu-3Bi solder; (g) low magnification; and (h) high magnification.

of 20°C. A triangular waveform with 0.1 Hz frequency and R = −1 strain ratio was used for the fatigue tests. The cycle loading was started from the tensile side. The fatigue failure was defined as 25% reduction of maximum tensile load.

In order to avoid the local deformation and stress concentration at the contact point induced by the conventional displacement-measuring device, a digital image measurement system was used in the present strain-controlled fatigue test. With a 50-mm

Table II. Mechanical Properties of Lead-Free Solders

Solder	Young's Modulus (GPa)	Yield Strength (MPa)	Tensile Strength (MPa)	True Fracture Ductility (D)	Hardness
Sn-3.5Ag	50	18.9	37.5	1.6	11.0 HV
Sn-3Ag-0.5Cu	54	25.3	50.6	1.23	13.3 HV
Sn-3Ag-0.5Cu-1Bi	52	50.6	72.6	0.8	18.3 HV
Sn-3Ag-0.5Cu-3Bi	53	38.1	91.3	0.36	28.6 HV
Sn	41.6[10]	—	—	—	3.9 HB[10]
Bi	32[10]	—	—	—	7 HB[10]

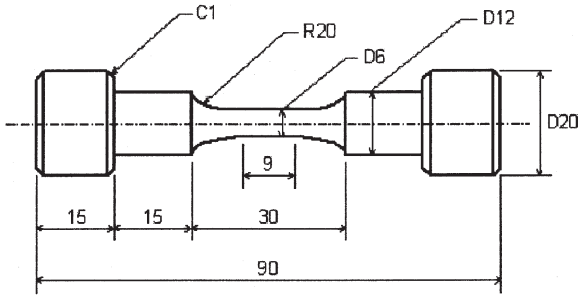

Fig. 2. Low-cycle fatigue specimen geometry (dimensions in mm).

CCD camera lens and 200-mm working distance (distance between the specimen and the lens), the field of observation is approximately 10 mm in the longitudinal direction of the specimen, covering the entire gage length. The smallest displacement that this system can detect is 8 μm. More details about this noncontact digital image measurement system have been given in the previous work.[7] During the fatigue test, cracks on the surface of the specimen were observed by using a replication technique.[13] After failure, the longitudinal cross sections of the specimens were examined in an SEM.

RESULTS AND DISCUSSION

LCF Behavior

Cyclic Flow Behavior

Both the load signal from the load cell and the displacement signal from the digital image system were recorded in a personal computer and then were used for calculating cyclic stress and strain in each cycle. Stress-strain hysteresis loops of four solders at the first cycle for 1.5% total strain range are shown in Fig. 3. For the same total strain range, the stress range increased while the plastic strain range decreased with increasing amounts of Bi. These results correspond to a greater tensile strength and microhardnesses measured for Sn-Ag-Cu-Bi alloys. For Sn-3Ag-0.5Cu, the stress range and plastic strain range are not much different when compared with those of Sn-3.5Ag. The plastic strain range increased with the applied total strain range but did not vary with the number of cycles for alloys investigated, in agreement with the behavior reported by Guo et al.[14] In the present study, a small decrease in plastic strain range for a few initial cycles was observed in the case of Sn-3Ag-0.5Cu-3Bi solder, particularly at high strain ranges.

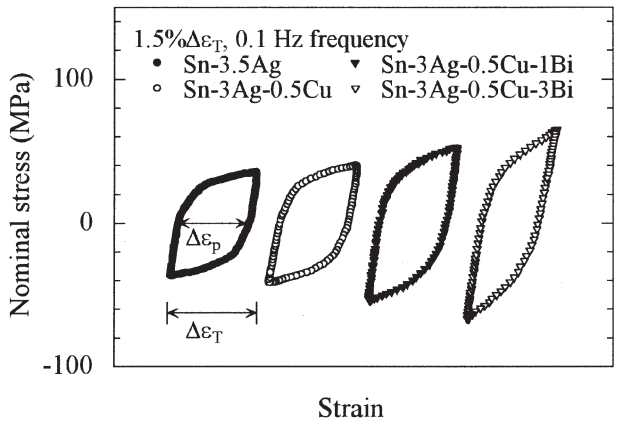

Fig. 3. Cyclic stress-strain hysteresis loops at the beginning of fatigue tests.

The relationships between stress amplitude (one-half of the stress range) and number of cycles for all solders for different total strain ranges are shown in Fig. 4. Cyclic softening was observed for Sn-3.5Ag, Sn-3Ag-0.5Cu, and Sn-3Ag-0.5Cu-1Bi from the beginning of the tests. The stress amplitude exhibited by Sn3Ag-0.5Cu was marginally higher than that for Sn-3.5Ag; however the rate of decrease of stress amplitude was nearly identical. On the other hand, Sn-3Ag-0.5Cu-1Bi exhibited a higher stress amplitude with a relatively faster rate of softening compared to the other two alloys. The alloy Sn-3Ag-0.5Cu-3Bi showed initial hardening, which was more prominent at higher strain ranges.

The observed cyclic flow behavior is consistent with the microstructural features of the alloys. The initial rapid decrease followed by a slower rate of decrease of stress amplitude in Sn-3.5Ag has been attributed to the development of extensive surface cracking along the β-Sn dendrite boundaries and their linking up and propagation transgranularly through the Sn-Ag eutectic phase and intergranularly along Sn-dendrite or subgrain boundaries at this test frequency.[15] The presence of Cu in Sn-3Ag-0.5Cu solder introduces Cu_6Sn_5 precipitates in the eutectic phase, and this is responsible for the slightly higher stress amplitude observed for this material compared to Sn-3.5Ag. There were no other significant differences in their cyclic flow behavior. There is a considerable increase in the stress amplitude for Sn-3Ag-0.5Cu-1Bi solder compared to Bi-free solders; however, the pattern of variation of stress amplitude with cycling is again a rapid de-

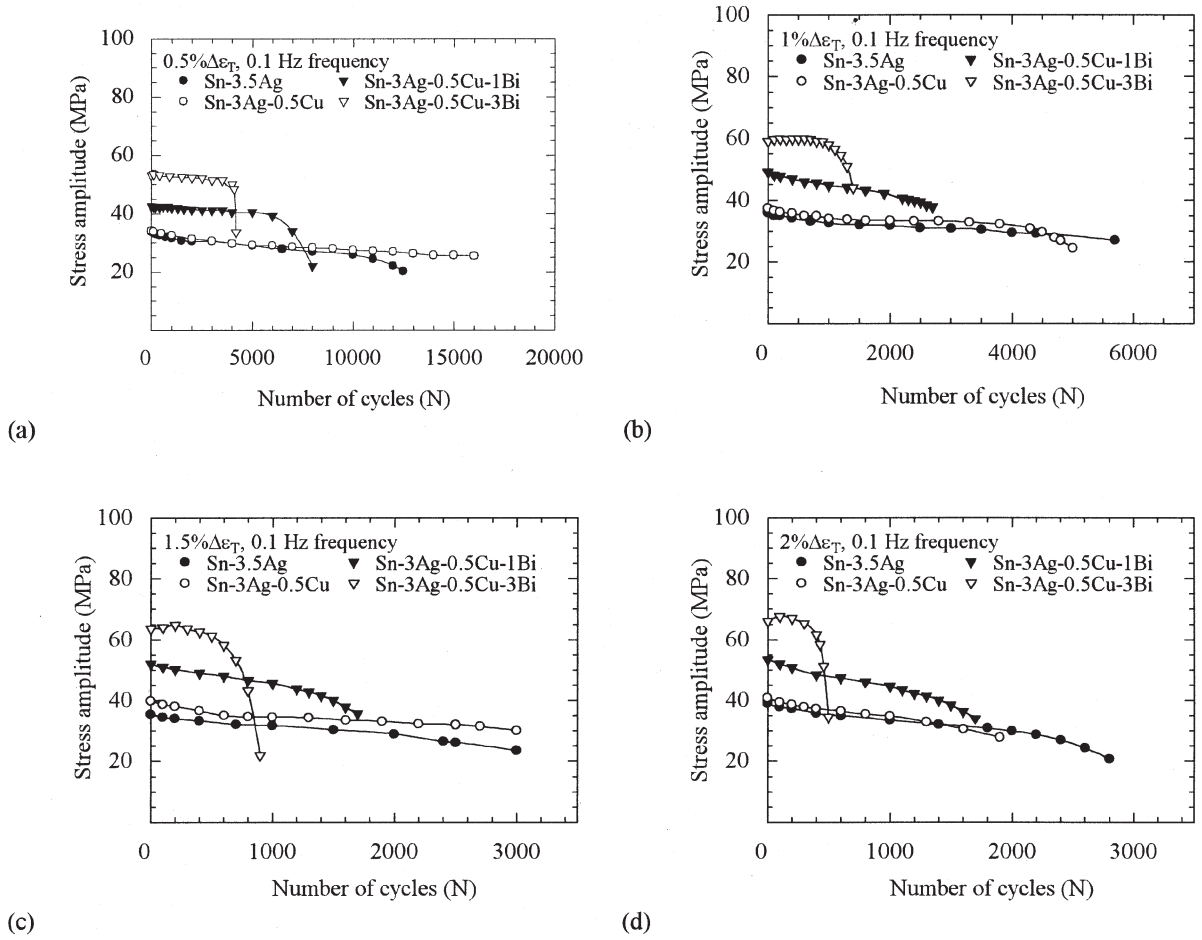

Fig. 4. Relationship between stress amplitudes and number of cycles.

crease followed by a slow rate of softening before instability sets in. The addition of 1% Bi in this solder would essentially go in solid solution in β-Sn at room temperature and leads to strengthening of this phase. As β-Sn comprises about 90% of the volume fraction in this material, solid solution strengthening by Bi is expected to increase stress amplitude and decrease plastic strain range as observed.

The cyclic response of Sn-3Ag-0.5Cu-3Bi is somewhat different than the other solders. Apart from the higher stress response, there is clearly initial hardening observed, particularly at large strain amplitudes, followed by softening. This material, in addition to solid solution hardening of β-Sn dendrites, contains precipitates of Bi. The initial hardening, therefore, is attributed to the presence of Bi precipitates and arises from the interaction of dislocations with these precipitates. The presence of Bi precipitates in β-Sn dendrites makes deformation of this material difficult compared to other solders and results in higher stress response and lower plastic strains for the same applied total strains.

Cyclic Stress-Strain Relationships

A plastic strain range was not influenced significantly by cycling. Plastic strain ranges, therefore, are plotted against stress ranges on the log-log scale in Fig. 5. The data could be fitted by a straight line, which is represented in the following form of equation:

$$\Delta\sigma = A\Delta\varepsilon_p^{\beta} \quad (1)$$

where $\Delta\sigma$ is the stress range, $\Delta\varepsilon_p$ is the plastic strain range obtained from the width of hysteresis loop, A is the cyclic strength coefficient, and β is the cyclic

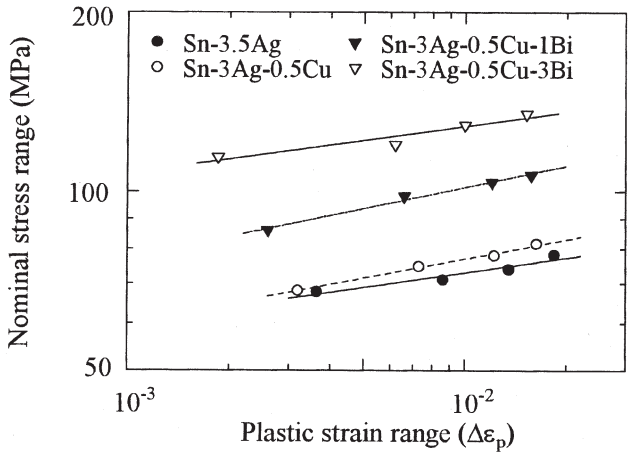

Fig. 5. Relationship between nominal stress range and plastic strain range.

strain-hardening exponent. Sn-3.5Ag had the lower cyclic strain-hardening coefficient (A) of 107.4, while Sn-3Ag-0.5Cu-3Bi had the highest of 185.5. For all solders, the cyclic strain-hardening exponents (β) are basically similar, i.e., in the range 0.08–0.1.

S–N Curves

It is well known that the relationship between plastic strain range and number of cycles to failure follows the Coffin–Manson relationship.[16,17]

$$\Delta\varepsilon_p N_f^{\alpha} = \theta \quad (2)$$

where $\Delta\varepsilon_p$ is the plastic strain range, N_f is the fatigue life, α is the fatigue ductility exponent, and θ is the fatigue ductility coefficient. The Coffin–Manson relationships for all solders are shown in Fig. 6. The fatigue ductility exponent (α) and fatigue ductility coefficient (θ), obtained by the least-squares method, are summarized in Table III. All solders obey the Coffin–Manson relationship with correlation coefficients of 0.97–0.99.

The addition of Cu does not significantly affect the fatigue behavior of eutectic Sn-Ag solder, in agreement with earlier studies.[4,5] The addition of Bi leads to a significant decrease in fatigue life. It has been reported that the fatigue life of Sn-3.5Ag-Bi could be correlated with true fracture ductility.[5] Therefore, the true fracture ductility (D) of the present solders was calculated from tensile tests results as follows:

$$D = \ln[100/(100 - q)] \quad (3)$$

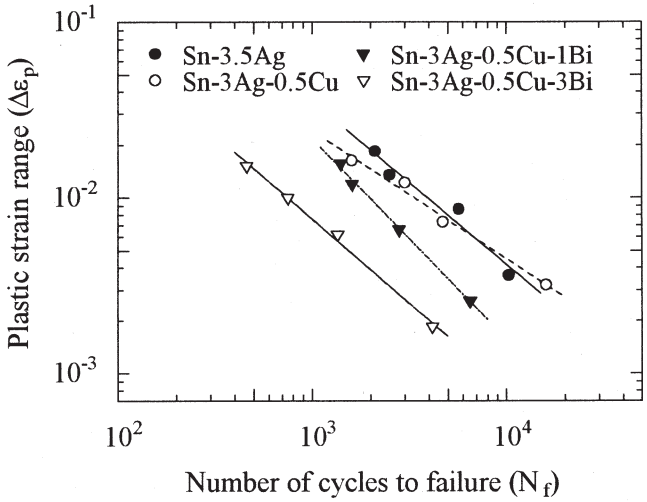

Fig. 6. Relationship between plastic strain range and number of cycles to failure.

Table III. Coffin–Mansion Parameters of Solders

Coffin–Manson Relationship	α	θ
Sn-3.5Ag	0.93	21.9
Sn-3Ag-0.5Cu	0.73	3.7
Sn-3Ag-0.5Cu-1Bi	1.14	57
Sn-3Ag-0.5Cu-3Bi	0.96	5.7

where q is the percent reduction of cross-sectional area at fracture:

$$q = \frac{A_0 - A_f}{A_0} \times 100 \quad (4)$$

where A_0 is the original cross-sectional area and A_f is the cross-sectional area at fracture. The true fracture ductility (D) of solders is given in Table II. The ductility normalized plastic strain range ($\Delta\varepsilon_p/2D$) was plotted with number of cycles to failure on the log-log scale, as shown in Fig. 7 for all the solders. All the results lie on a common stright line. The fatigue life of the present solders is dominated by the fracture ductility and can be described by the ductility-modified Coffin–Manson's relationship as follows:

$$(\Delta\varepsilon_p/2D)N_f^{\alpha} = \theta \quad (5)$$

where α is 1.07 and θ is 13.

LCF Mechanisms

Crack Initiation

According to the stress-number of cycles relationship, the solders studied were divided into two groups, i.e., no cyclic hardening-behavior group (Sn-3.5Ag, Sn-3Ag-0.5Cu, and Sn-3Ag-0.5Cu-1Bi) and cyclic hardening-behavior group (Sn-3Ag-0.5Cu-3Bi). The initiation of cracks was observed on the surface of specimens by a replication technique. The SEM micrographs of replica films of Sn-3.5Ag[18] and Sn-3Ag-0.5Cu-3Bi specimens tested at 1% $\Delta\varepsilon_T$ are shown in Fig. 8. It should be noted that replica film shows a reverse image of the specimen surface, i.e., a crack is represented by a fin on the replica film. For no cyclic hardening behavior groups of solders, cracks were mostly observed at the boundaries of dendrite phases (area A) in the early stage of fatigue tests, which linked up and propagated with an increasing number of cycles. On the other hand, intergranular cracks initiated along dendrite bound-

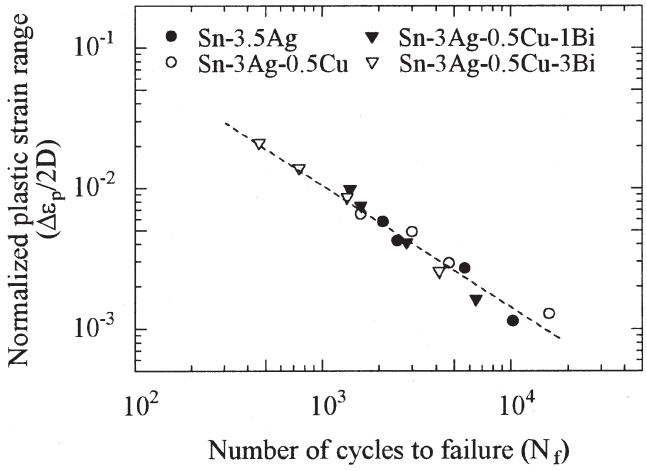

Fig. 7. Relationship between plastic strain ranges normalized by true fracture ductility and number of cycles to failure.

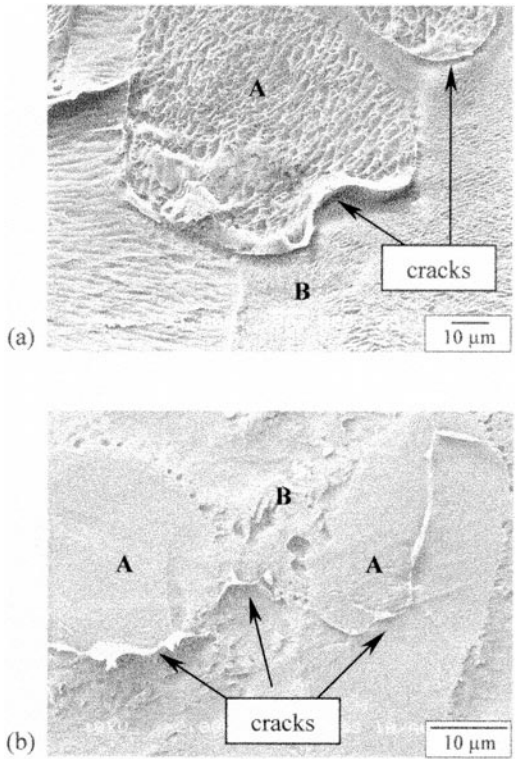

Fig. 8. SEM micrographs of replica films of the surface of: (a) Sn-3.5Ag specimen tested at 1% $\Delta\varepsilon_T$, 800 cycles;[18] and (b) Sn-3Ag-0.5Cu-3Bi specimen tested at 1% $\Delta\varepsilon_T$, 800 cycles. A and B represent the dendrite phase and eutectic phase, respectively (load direction is vertical).

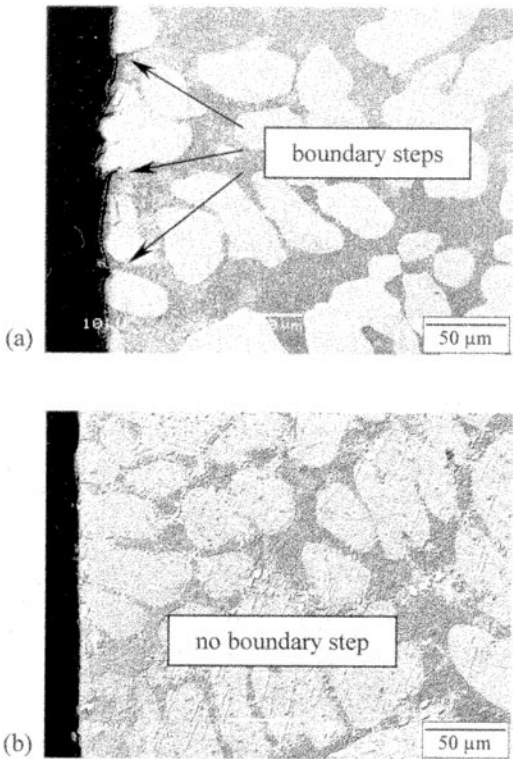

Fig. 9. SEM micrographs of the longitudinal cross section of the failed specimens tested at 1% $\Delta\varepsilon_T$: (a) Sn-3Ag-0.5Cu and (b) Sn-3Ag-0.5Cu-3Bi (load direction is vertical).

aries and subgrain boundaries in Sn-3Ag-0.5Cu-3Bi, the solder that exhibited initial hardening behavior. This extensive cracking leads to a decrease in stress amplitude due to a decrease in load bearing area for Sn-3.5Ag, Sn-3Ag-0.5Cu, and Sn-3Ag-0.5Cu-1Bi, as shown in Fig. 4b. Though cracking was also observed in Sn-3Ag-0.5Cu-3Bi, the incidence of cracking in this material was less compared to other solders. The increase in stress (i.e., initial hardening) could result from hardening due to dislocation-dislocation, dislocation-precipitate interactions due to the presence of Bi precipitates in this solder. This hardening more than compensates for the decrease in stress due to cracking resulting in reduced load bearing area.

Due to differences in the strength of the dendrite phase and the eutectic phase, steps would be created along the Sn dendrites due to deformation for the solder without Bi precipitates in dendrites. These steps lead to formation of cracks along the dendrite boundaries due to stress concentration effects. The presence of Bi precipitates in Sn-3Ag-0.5Cu-3Bi probably reduces the strength difference between the dendrites and the eutectic phase, and virtually no steps were seen in this solder (Fig. 9). The crack initiation process in Sn-3Ag-0.5Cu-3Bi solder occurred by a mixed mode involving dendrite boundaries and subgrain boundaries in the dendrites. The formation of these subgrains and their role in fatigue deformation are discussed elsewhere.[15,18] It has been pointed out that subgrains due to polygonization rather than recrystallized grains are more likely to form in a high stacking fault energy material such as Sn. The formation of cavities at the boundaries of subgrains formed in the dendrite phase of Sn-3Ag-0.5Cu-3Bi solder is evident in Fig. 10. Evidence of sliding of the boundaries is also shown in the figure. Therefore, the cavities at these boundaries originated due to boundary sliding. No sliding of dendrite boundaries was observed, probably due to the nature of such boundaries. The presence of Bi precipitates at subgrain boundaries might have facilitated the formation of these cavities, which consequently link up to form cracks.

Crack Propagation

The LCF deformation leads to the formation of numerous surface cracks. With an increasing number of cycles, the number of cracks on the surface of the specimen increased; however, their sizes were limited to the size of the dendrite phase. Growth of these multiple cracks in the depth direction was also limited (approximately 5–10 μm), which means that the multiple cracks were "shallow surface cracks." Such cracks have also been observed in Sn-3.5Ag over a wide range of frequencies.[15] Examples of these surface cracks (arrows) for solders Sn-3Ag-0.5Cu and Sn-3Ag-0.5Cu-3Bi are shown in Fig. 11. After a certain number of cycles, some of the surface cracks eventually linked-up to form

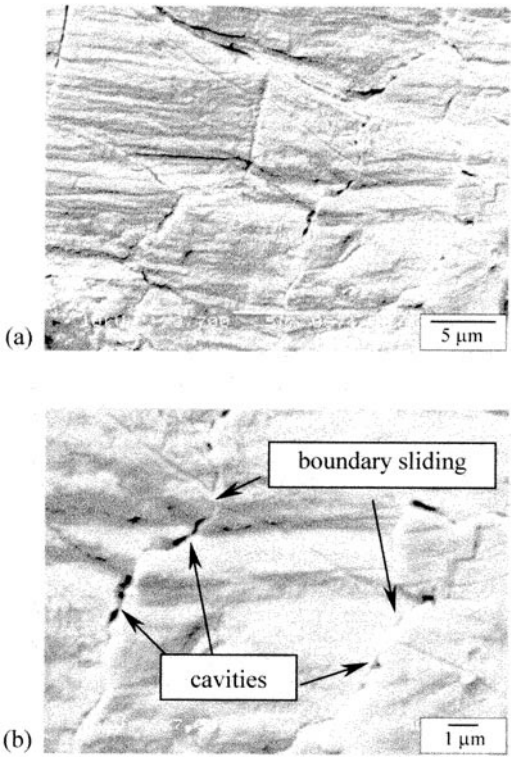

Fig. 10. SEM micrographs of the surface of the failed Sn-3Ag-0.5Cu-3Bi specimen tested at 1% $\Delta\varepsilon_T$: (a) low magnification and (b) high magnification (load direction is vertical).

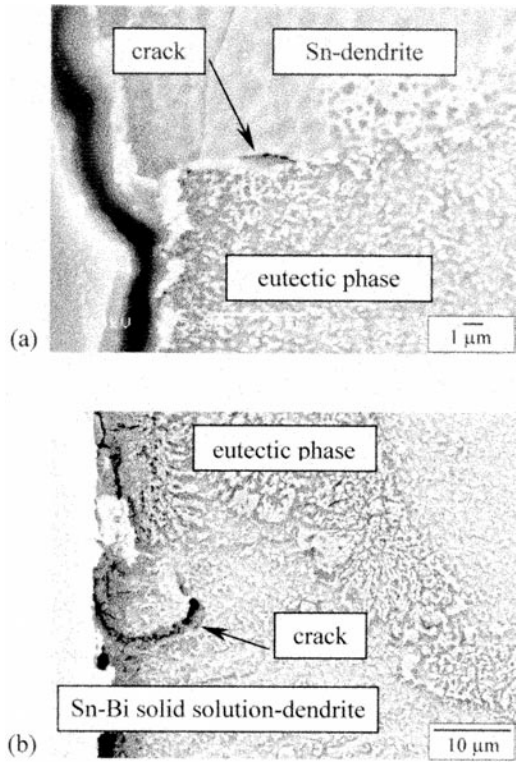

Fig. 11. SEM micrographs of the surface crack on the longitudinal cross section of the specimen tested at 1% $\Delta\varepsilon_T$: (a) Sn-3Ag-0.5Cu and (b) Sn-3Ag-0.5Cu-3Bi (load direction is vertical).

larger cracks. Link-up of surface cracks to form large cracks involved both transgranular (through the eutectic phase) and intergranular (along the dendrite boundaries) processes. In some cases, link-up also involved transgranular mode fracture through the dendrite phase, possibly along subgrain boundaries. Examples of this link-up are shown in Fig. 12. The propagation of these cracks through the specimen essentially involved similar processes as the link-up cracks (Fig. 13). Higher magnification micrographs in Fig. 13 show that propagation through the dendrites occurred along subgrain boundaries.

Fatigue life was reduced with the addition of Bi. It is suggested that lower ductility and lower life observed with Bi addition arise due to strengthening of the Sn-dendrite with solid solution of Bi as well as precipitates. The presence of Bi precipitates in Sn-3Ag-0.5Cu-3Bi leads to the formation of cavities (Fig. 14) and also probably contributes to a decrease in fatigue life. The high response stresses observed with Bi addition would be another reason for the observed reduced fatigue life.

CONCLUSIONS

Isothermal LCF behavior and mechanisms of crack initiation and propagation in Sn-3.5Ag, Sn-3Ag-0.5Cu, Sn-3Ag-0.5Cu-1Bi, and Sn-3Ag-0.5Cu-3Bi solders have been studied at 20°C with a constant frequency of 0.1 Hz. The main conclusions obtained are summarized as follows.

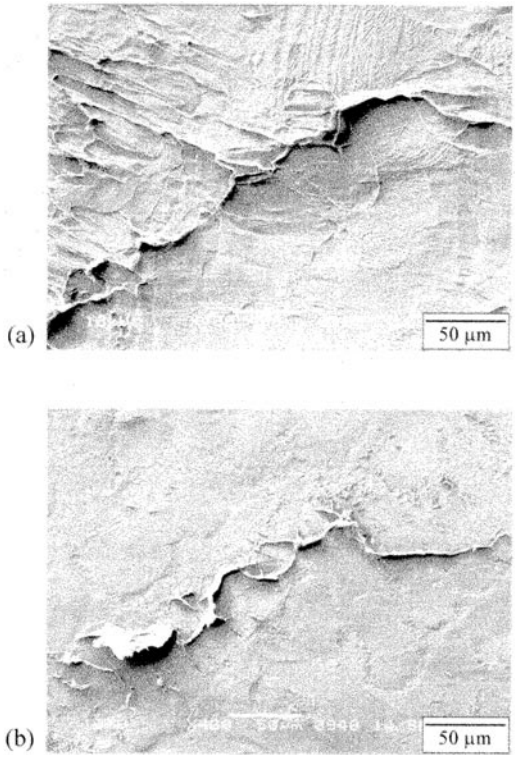

Fig. 12. SEM micrographs of replica films of the surface of specimens tested up to 800 cycles, at 1% $\Delta\varepsilon_T$: (a) Sn-3.5Ag[18] and (b) Sn-3Ag-0.5Cu-3Bi (load direction is vertical).

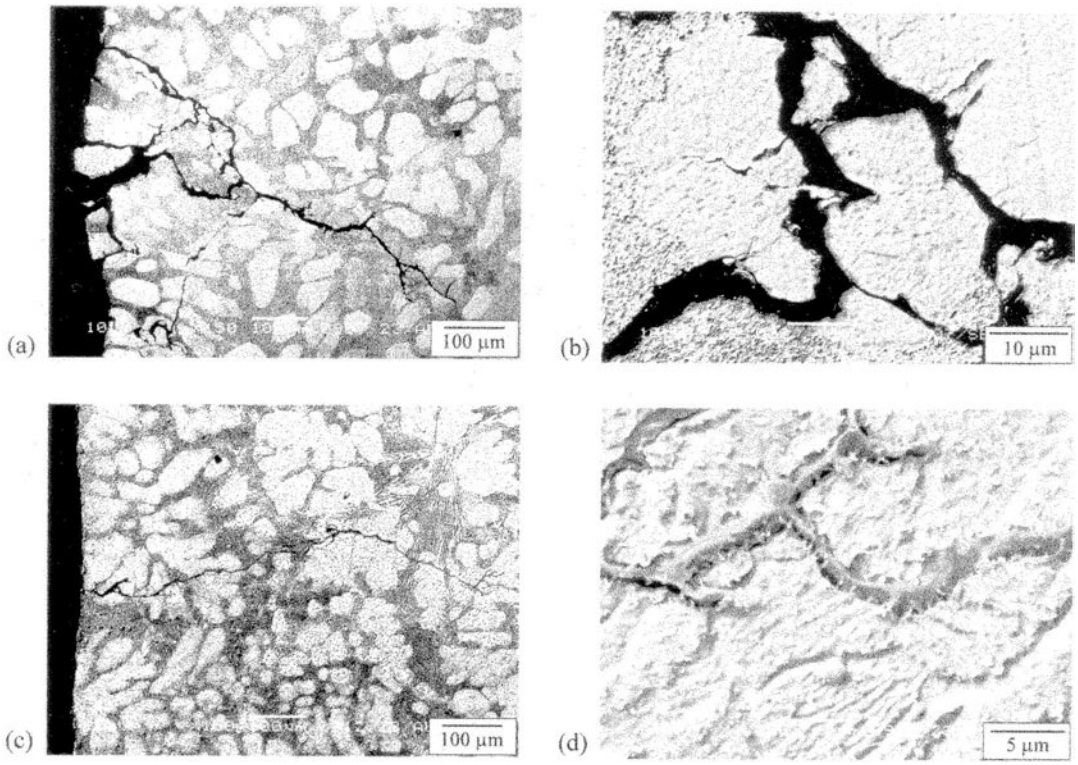

Fig. 13. SEM micrographs of the longitudinal cross section of: the Sn-3Ag-0.5Cu specimen tested at 1% $\Delta\varepsilon_T$, (a) low magnification and (b) high magnification, and Sn-3Ag-0.5Cu-3Bi specimen tested at 1% $\Delta\varepsilon_T$, (c) low magnification and (d) high magnification (load direction is vertical).

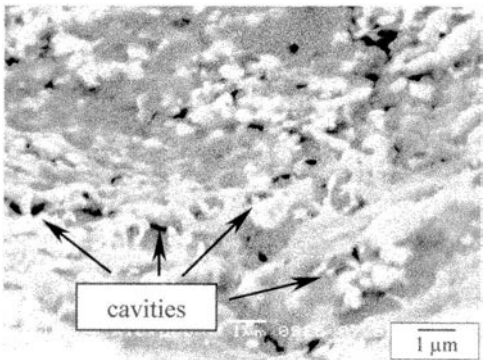

Fig. 14. SEM micrographs of cavities observed on the fracture surface of Sn-3Ag-0.5Cu-3Bi specimen tested at 1% $\Delta\varepsilon_T$.

- For Sn-3.5Ag, Sn-3Ag-0.5Cu, and Sn-3Ag-0.5Cu-1Bi solders, the pattern of variation of stress amplitude with cycling showed a rapid decrease followed by a slow rate of softening before instability sets in. The surface cracking, link-up, and propagation due to cycling contributed to the reduction in stress amplitude. On the other hand, Sn-3Ag-0.5Cu-3Bi exhibited initial hardening followed by softening at high strain ranges. The initial hardening is considered to arise from the interaction of dislocations with Bi-precipitates formed in dendrite phase.
- The addition of Cu does not significantly affect the fatigue life of eutectic Sn-Ag solder. However, the fatigue life was significantly reduced with the amount of the addition of Bi. The LCF behavior of all solders followed the Coffin–Manson equation. The fatigue life of the solders studied is dominated by the fracture ductility and can be described by the ductility modified Coffin–Manson's relationship.
- Multiple surface cracks predominantly initiated in an intergranular manner along the dendrite boundary steps for Sn-3.5Ag, Sn-3Ag-0.5Cu, and Sn-3Ag-0.5Cu-1Bi solders, and along both the dendrite boundaries and subgrain boundaries in dendrite phases for Sn-3Ag-0.5Cu-3Bi solder.
- The link-up of surface cracks and the propagation of cracks inside the specimen occurred both transgranularly through the eutectic phases and intergranularly along the dendrite boundaries or subgrain boundaries.

ACKNOWLEDGEMENTS

The authors thank T. Ori, Oki Electric Industry Co., Ltd., for supplying the solder materials used in this work, and Dr. S.L. Mannan for many fruitful discussions.

REFERENCES

1. S.K. Kang and A.K. Sarkhel, *J. Electron. Mater.* 23, 701 (1994).
2. F. Hua and J. Glazer, *Design and Reliability of Solders and Solder Interconnections*, eds. R.K. Mahidhara, D.R. Frear, S.M.L. Sastry, K.L. Liaw, and W.L. Winterbottom (Warrendale, PA: TMS Society, 1997), pp. 65–74.
3. M. McCormack and S. Jin, *JOM* 45, 36 (1993).
4. Y. Kariya and M. Otsuka, *J. Electron. Mater.* 27, 1229 (1998).

5. Y. Kariya and M. Otsuka, *J. Electron. Mater.* 27, 866 (1998).
6. R.S. Whitelaw, R.W. Neu, and D.T. Scott, Trans. *ASME, J. Electron. Packaging* 121, 99 (1999).
7. C. Kanchanomai, S. Yamamoto, Y. Miyashita, Y. Mutoh, and A.J. McEvily, *Int. J. Fatigue* 24, 57 (2002).
8. T. Lyman, ed., *Metals Handbook,* 8th ed. (Metals Park, OH: ASM, 1973), vol. 8, pp. 256, 273, and 299.
9. X.Q. Shi, H.L.J. Pang, W. Zhou, and Z.P. Wang, *Adv. Electronic Packaging,* ASME EEP 26-1, 551 (1999).
10. W.H. Cubberly, ed., *Metals Handbook,* 9th ed. (Metals Park, OH: ASM, 1979), vol. 2, pp. 618 and 719.
11. ASTM Standards, *ASTM E606: Standard Practice for Strain-Controlled Fatigue Testing* (Philadelphia: ASTM, 1998), vol. 03.01, pp. 525–39.
12. E.C. Cutiongco, S. Vaynman, M.E. Fine, and D.A. Jeannotte, *Trans. ASME, J. Electron. Packaging* 112, 110 (1990).
13. ASTM Standards, *ASTM E1351-96: Standard Practice for Production and Evaluation of Field Metallographic Replicas* (Philadelphia: ASTM, 1998), vol. 03.01, pp. 850–854.
14. G. Guo, E.C. Cutiongco, L.M. Keer, and M.E. Fine, *Trans. ASME, J. Electron. Packaging* 114, 145 (1992).
15. C. Kanchanomai, Y. Miyashita, Y. Mutoh, and S.L. Mannan, *Mater. Sci. Eng. A* (submitted).
16. L.F. Coffin, Jr., *Trans. ASME* 76, 931 (1954).
17. S.S. Manson, *Heat Transfer Symp.* (Ann Arbor: University of Michigan Press, 1953), pp. 9–76.
18. C. Kanchanomai, Y. Miyashita, and Y. Mutoh, *J. Electron. Mater.,* 31, 142 (2002).